

## Effect of temperature and humidity on the sensing performance of TiO<sub>2</sub> nanowire-based ethanol vapor sensors

Shooshtari, Mostafa; Salehi, Alireza; Vollebregt, Sten

**DOI**

[10.1088/1361-6528/abfd54](https://doi.org/10.1088/1361-6528/abfd54)

**Publication date**

2021

**Document Version**

Final published version

**Published in**

Nanotechnology

**Citation (APA)**

Shooshtari, M., Salehi, A., & Vollebregt, S. (2021). Effect of temperature and humidity on the sensing performance of TiO<sub>2</sub> nanowire-based ethanol vapor sensors. *Nanotechnology*, 32(32), 1-13. Article 325501. <https://doi.org/10.1088/1361-6528/abfd54>

**Important note**

To cite this publication, please use the final published version (if applicable). Please check the document version above.

**Copyright**

Other than for strictly personal use, it is not permitted to download, forward or distribute the text or part of it, without the consent of the author(s) and/or copyright holder(s), unless the work is under an open content license such as Creative Commons.

**Takedown policy**

Please contact us and provide details if you believe this document breaches copyrights. We will remove access to the work immediately and investigate your claim.

PAPER • OPEN ACCESS

## Effect of temperature and humidity on the sensing performance of TiO<sub>2</sub> nanowire-based ethanol vapor sensors

To cite this article: Mostafa Shooshtari *et al* 2021 *Nanotechnology* **32** 325501

View the [article online](#) for updates and enhancements.



**RM5**  
Our confocal  
Raman Microscope.  
Your Research. Our Expertise.

EDINBURGH  
INSTRUMENTS

edinst.com

# Effect of temperature and humidity on the sensing performance of TiO<sub>2</sub> nanowire-based ethanol vapor sensors

Mostafa Shoostari<sup>1</sup> , Alireza Salehi<sup>1</sup> and Sten Vollebregt<sup>2</sup> 

<sup>1</sup>Department of Electrical Engineering, K N Toosi University of Technology, Tehran, Iran

<sup>2</sup>Department of Microelectronics, Delft University of Technology, Delft, The Netherland

E-mail: [s.vollebregt@tudelft.nl](mailto:s.vollebregt@tudelft.nl)

Received 19 January 2021, revised 30 March 2021

Accepted for publication 29 April 2021

Published 17 May 2021



CrossMark

## Abstract

In this paper, we study the influence of two key factors, temperature, and humidity, on gas sensors based on titanium dioxide nanowires synthesized at 4 different temperatures and with different morphology. The samples' structure are investigated using SEM, XRD and FTIR analysis. The effects of humidity and temperature are studied by measuring the resistance and gas response when exposed to ethanol. At room temperature, we observed a 15% sensitivity response to 100 ppm of ethanol vapor and by increasing the operating temperature up to 180 °C, the response is enhanced by two orders of magnitude. The best operating temperature for the highest gas response is found to be around 180 °C. Also, it was observed that every nanowire morphology has its own optimum operating temperature. The resistance of sensors is increased at higher Relative Humidity (RH). Besides, the response to ethanol vapor experiences a gradual increase when the RH rises from 10% to 60%. On the other hand, from 60% to 90% RH the gas response decreases gradually due to different mechanisms of interaction of the TiO<sub>2</sub> with H<sub>2</sub>O and ethanol molecules.

Supplementary material for this article is available [online](#)

Keywords: titanium dioxide, ethanol, vapor sensor, humidity, cross-sensitivity

(Some figures may appear in colour only in the online journal)


## 1. Introduction

Titanium dioxide (TiO<sub>2</sub>) is an important metal oxide semiconductor (MOS) that is desirable for many applications, such as pigment [1], solar cells [2], optical waveguides [3], filters [4], and gas sensors [5]. Researchers present their properties via quantum confinement and surface effect by reducing the size of TiO<sub>2</sub> crystals to nanoscale dimensions [6, 7]. Controlling the morphology of TiO<sub>2</sub> crystals in nanostructures, such as nanowires and nanoparticles, can also affect its electrical properties such as sheet resistance [8]. TiO<sub>2</sub>

nanowire (NW-TiO<sub>2</sub>) can be prepared by several methods [9], as will be discussed in more detail in the next section.

NW-TiO<sub>2</sub> based gas sensors have received great attention due to their excellent sensing property to alcohol vapors such as butanol, ethanol and acetone [10, 11]. The finite carrier density and high surface-to-volume ratio are possible causes for the observed high sensitivity [12]. In general, TiO<sub>2</sub> gas sensors can mainly detect a gas because of the change in the electrical signal caused by the adsorption and reaction of the gas molecules on absorption sites on the surface. The change in the electrical property is the consequence of charge transfer between the sensing layer and the gas molecules [5, 13].

The gas sensing mechanism of metal-oxide gas sensors is related to the absorption sites and the number of oxygen atoms on the surface [13, 14]. Besides the analyte of interest, water vapor is normally present in the ambient environment

 Original content from this work may be used under the terms of the [Creative Commons Attribution 4.0 licence](#). Any further distribution of this work must maintain attribution to the author(s) and the title of the work, journal citation and DOI.

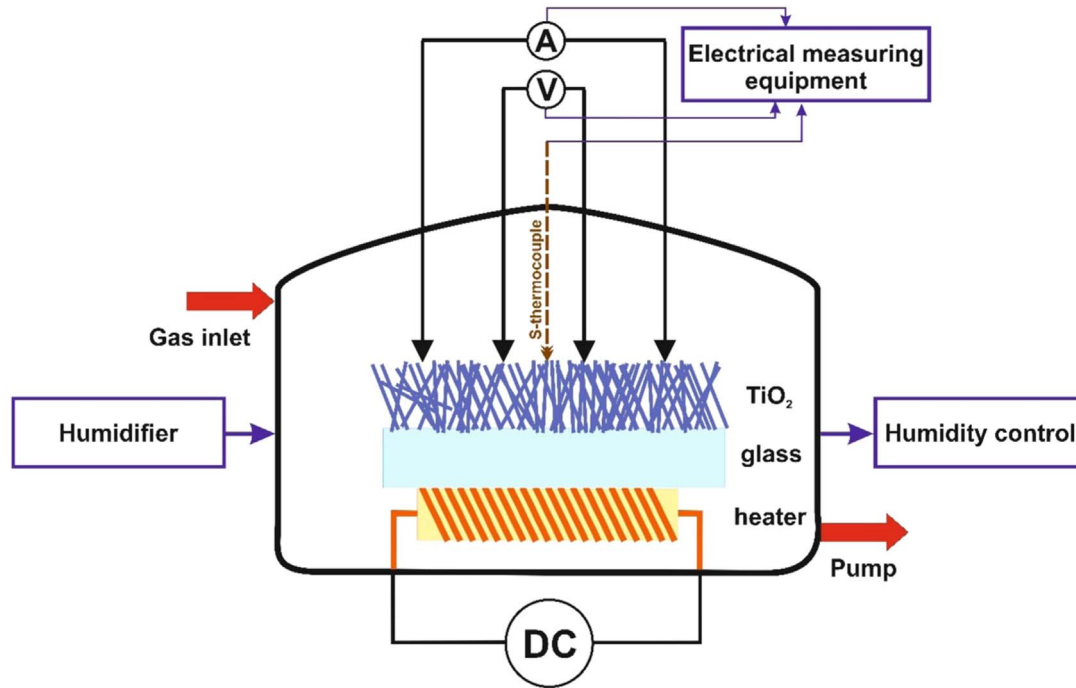


Figure 1. Schematic diagram of the measurement system.

[15]. Similar to reducing gases, water vapor is known to increase the conductance of semiconductor gas sensors [16]. The water molecule can affect both the gas-absorbing surface and the number of surface oxygen atoms.

On the other hand, increasing the operating temperature is a method often used to increase the sensitivity in metal-oxide gas sensors while the temperature can also help reduce the sensitivity to water. Despite its attractive features such as a higher sensitivity, this may lead to an unrepeatable gas response [17].

In this paper, the effects of temperature and humidity on the gas response of NW-TiO<sub>2</sub> based ethanol gas sensors are investigated. A possible explanation of the observed temperature and humidity effects are given, and the mechanism of interaction of the TiO<sub>2</sub> with H<sub>2</sub>O and ethanol molecules is proposed. Based on the obtained results, optimal growth and testing conditions of gas sensing to reduce the effect of humidity and temperature are discussed.

## 2. Experimental

### 2.1. NW-TiO<sub>2</sub> growth

A MOS sensor's sensitivity can be increased by using materials with nanostructures. To reduce the dimension of TiO<sub>2</sub> from three to zero, several methods have been proposed [18–21]. Recently, one-dimensional nanostructures such as NW-TiO<sub>2</sub>, have attracted much interest owing to their high surface-to-volume ratio and relatively easy and rapid synthesis for gas sensing [22–25]. To prepare the NW-TiO<sub>2</sub> for gas sensors, many techniques such as chemical vapor deposition (CVD) [26], microwave heating [27], laser ablation [28],

solution-liquid-solid [29], arc discharge [28], vapor-liquid-solid [30], and the hydrothermal method [31] have been developed. Among these, the hydrothermal method is well-known because it is a simple, controllable, safe, inexpensive, and novel approach. Also, hydrothermal synthesis does not require any physical template or catalyst materials that may cause contamination.

In this study, the growth of TiO<sub>2</sub> nanowires is performed using 0.3 molar titanium isopropoxide mixed with 0.1 molar ethanalamine in a magnetic stirrer for two hours. Next, 10 molar sodium hydroxide (NaOH) is added to the mixture and kept on the magnetic stirrer for an extra hour. Then, the solution is held at a temperature between 120 °C and 180 °C for 20 h. We define four samples A, B, C and D and expose them at temperatures of 120 °C, 140 °C, 160 °C, and 180 °C, respectively. This temperature range is required to form structures with different degrees of porosity. After this period, the solution is cooled down to room temperature. The obtained sediment is centrifuged and washed several times with distilled water and placed at 60 °C to dry for 24 h. Dried sediment is collected and added to a 0.1 molar hydrochloric acid (HCl) solution for one hour. The white colored sediment is collected by centrifugation and washed several times again with distilled water and ethanol (C<sub>2</sub>H<sub>6</sub>O) and dried at 100 °C for one hour. Finally, nanowire titanium dioxide is obtained by baking the sediment at 500 °C in the air for an extra hour.

### 2.2. Fabrication of devices for the measurements

Figure 1 shows the schematic diagram of the measurement system. The test set-up consists of a glass test chamber for sensors, two separate pipelines for entry and exit of water vapor and gas, and the electrical measurement equipment to

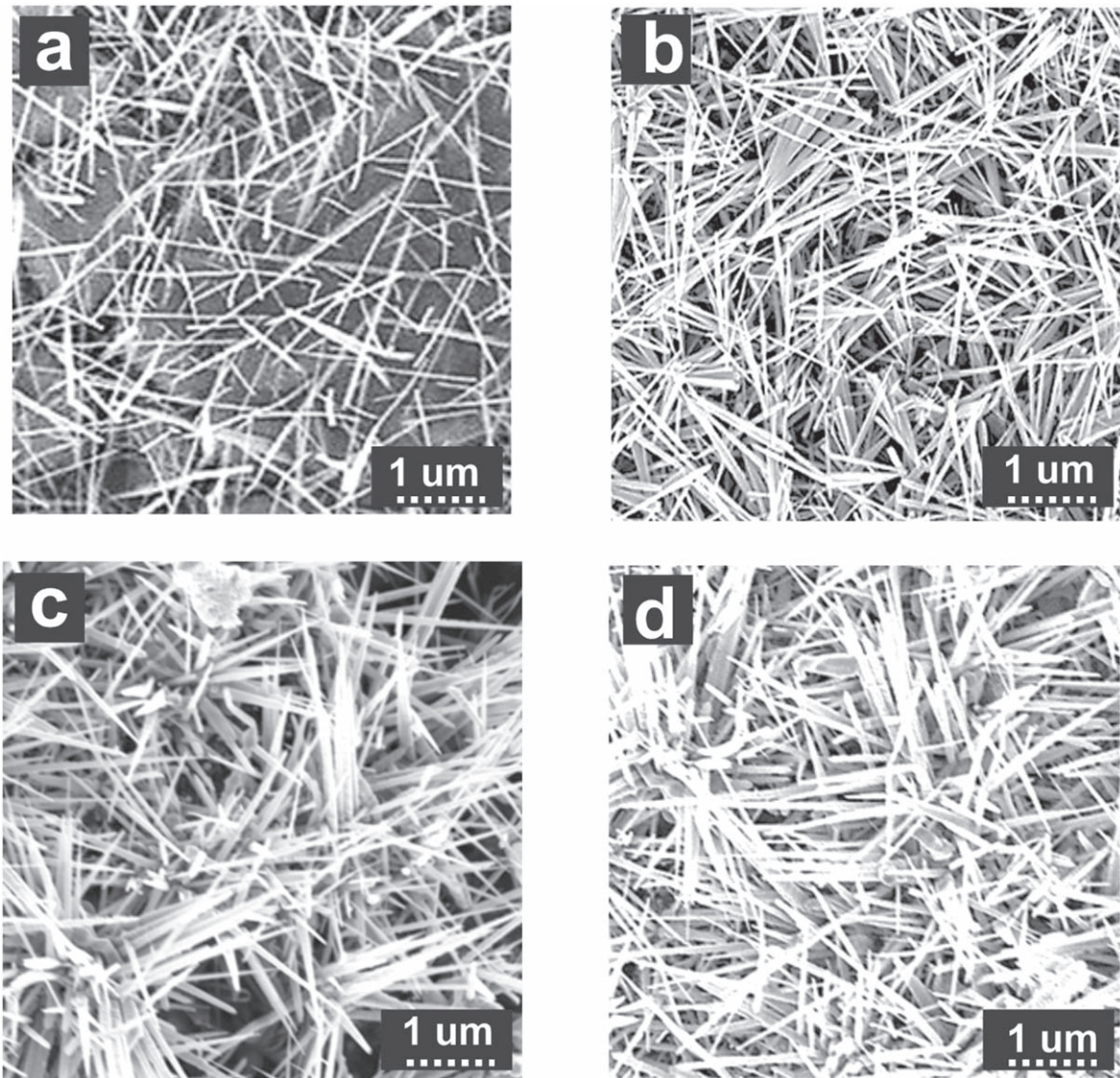


**Figure 2.** SEM images of the samples obtained at different temperatures: (a) sample A (120 °C), (b) sample B (140 °C), (c) sample C (160 °C), (d) sample D (180 °C).

acquire the electrical signals from the sensors. To measure conductivity via the 4-point probes method, a Keithley 238 source measure unit is used.

Relative humidity (RH) and temperatures inside the chamber are monitored during all experiments. A Samwon commercial humidity meter is also used to measure ambient humidity. The amount of humidity required for calibration is generated by a commercial ultrasonic humidifier JR model JRG. A 1.6 MHz oscillator with 100 V output voltage is designed for the humidifier. A silica gel is used to reduce the moisture content. The measurement operation is not carried out until the pump has worked for 12 h to obtain a stable RH in the test chamber. To ensure that the operating temperature of the sensor remains unchanged, the resulting chip is placed on a micro-heater. This micro-heater provides a tuneable temperature varying from room temperature up to 450 °C by applying a DC voltage. A thermocouple type S is placed on the sensor surface to measure the temperature.

The sensitivity factor of the NW-TiO<sub>2</sub> sensor is obtained using the measured current and voltage shown in figure 1. The resistance  $R$  of the sample in air and when exposed to the test gas is measured. The response factor of the sensors is then expressed by:

$$\text{Response} = \frac{R_a}{R_g}, \quad (1)$$

where  $R_a$  is the resistance of the sensor measured in air at room temperature and  $R_g$  is the resistance of the sensor in the presence of the test gas.

The sensors response were obtained at the presence of ethanol vapor at different concentrations which were provided by evaporating an exact amount of liquid ethanol, which was measured by a micro sampler, into the air chamber. A 5-litre air-filled glass container is utilized as the controlled atmosphere chamber. Ethanol (Merck/ 1.00983.1000) vapor is used as analyte. The evaporation of these liquids produces different

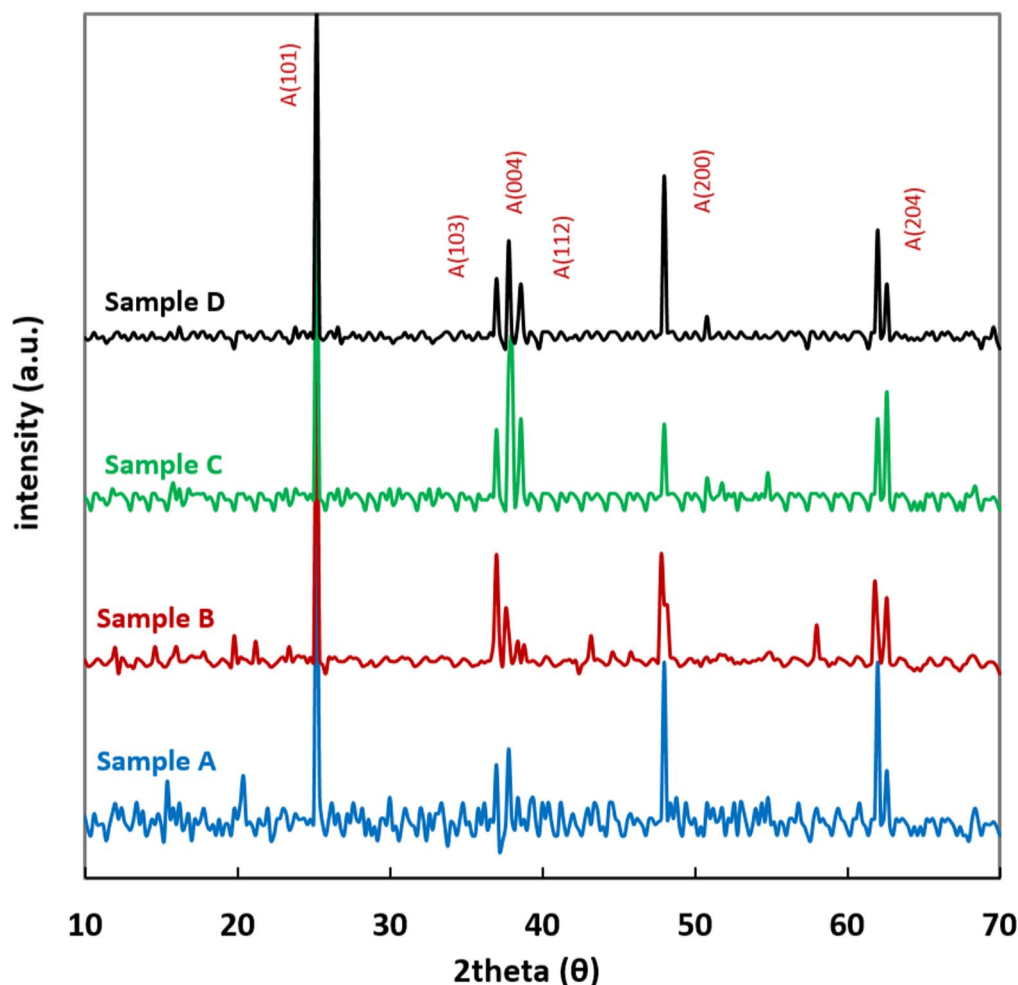


**Figure 3.** X-ray diffraction (XRD) pattern of synthesized structures for NW-TiO<sub>2</sub> samples obtained at different treatment temperatures: (a) sample A (120 °C), (b) sample B (140 °C), (c) sample C (160 °C), (d) sample D (180 °C). A(XXX) is Anatase (XXX).

**Table 1.** XRD Data of NW-TiO<sub>2</sub> samples.

Sample	2θ	FWHM (Radian)	βcosθ	A (nm)	d-spacing (Å)
Sample A	25°	0.002058	0.00200	69	3.6
	48°	0.001988	0.00181	77	1.9
Sample B	25°	0.001945	0.00189	73	3.6
	48°	0.001867	0.00170	82	1.9
Sample C	25°	0.001972	0.00182	72	3.6
	48°	0.001913	0.00174	80	1.9
Sample D	25°	0.001919	0.00187	74	3.6
	48°	0.001867	0.00170	82	1.9

ethanol concentration levels, from 5 to 100 ppm, in the closed chamber.

### 3. Result and discussion

#### 3.1. Characterization

The structure and phase identification of NW-TiO<sub>2</sub> samples are investigated with scanning electron microscopy (SEM),

x-ray diffractometry (XRD, Inel, EQUINOX3000) and Fourier-transform infrared (FTIR, JASCO, 460 Plus) spectroscopy. Before SEM observation, the samples are coated with a 10 nm layer of gold using a sputter coater to minimize the charging effect on the sample surface. In the XRD equipment monochromatic optic Kα1 or Kα1/2 are used ( $\lambda = 0.15405$  nm, at 40 kV and 25 mA).

Figures 2(a)–(d) shows the titania nanowires formed in each sample. The manufacture nanowires are 10–20 micrometer in length and 30–60 nanometer in diameter. The nanowires have a higher surface area than the other crystalline structures [32]. We note that the hydrothermal method of synthesis applied to the NW-TiO<sub>2</sub> samples provides conditions for controlling the size of the nanowires through controlling the synthesis temperature.

According to the SEM images, NW-TiO<sub>2</sub> samples are successfully fabricated by the applied hydrothermal method. As can be seen, the NW-TiO<sub>2</sub> are porous and clean with no apparent contamination attached to the wires. In addition, some nanowires seem to be wider than others. This small size difference is attributed to the preparation process of the SEM sample where the Au coating can fuse NW which are adjacent. This also prevents us from accurately determining the

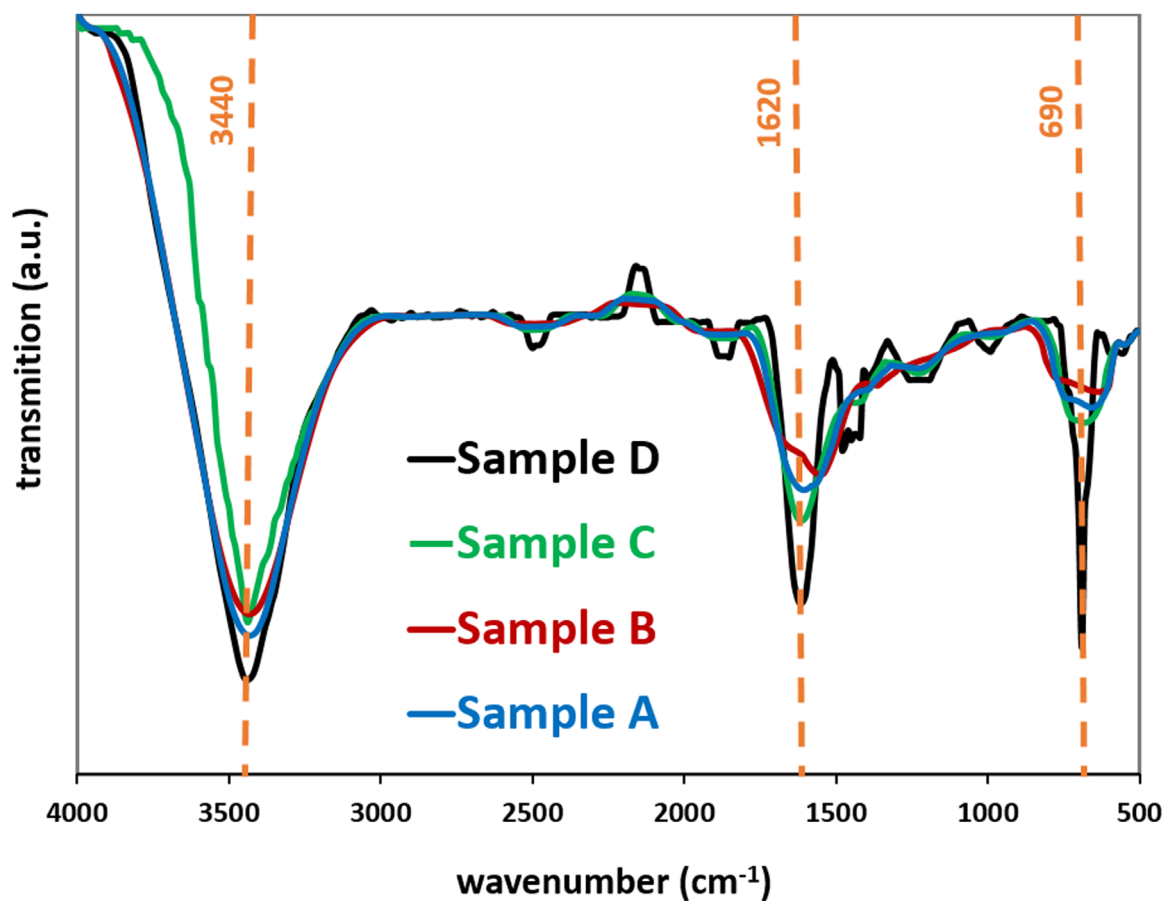


**Figure 4.** Fourier-transform infrared (FTIR) spectra of synthesized structures for NW-TiO<sub>2</sub> samples obtained at different treatment temperatures: (a) sample A (120 °C), (b) sample B (140 °C), (c) sample C (160 °C), (d) sample D (180 °C).

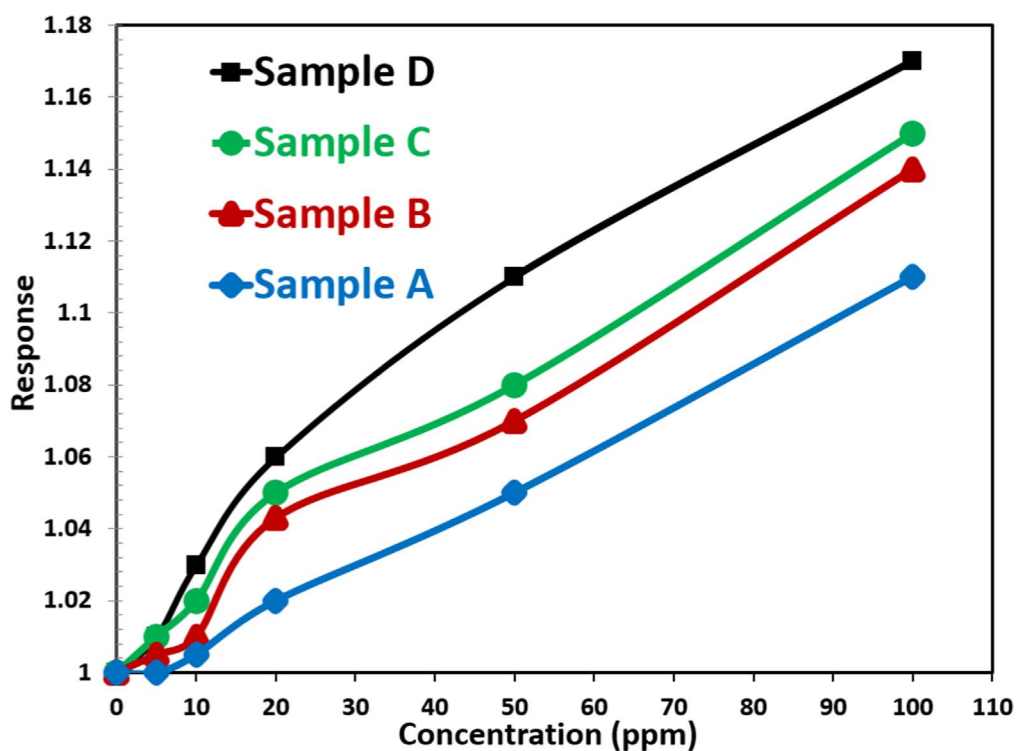


**Figure 5.** Response profiles of ethanol vapor sensors based on NW-TiO<sub>2</sub> samples upon exposure to different concentrations of ethanol vapor at room temperature.

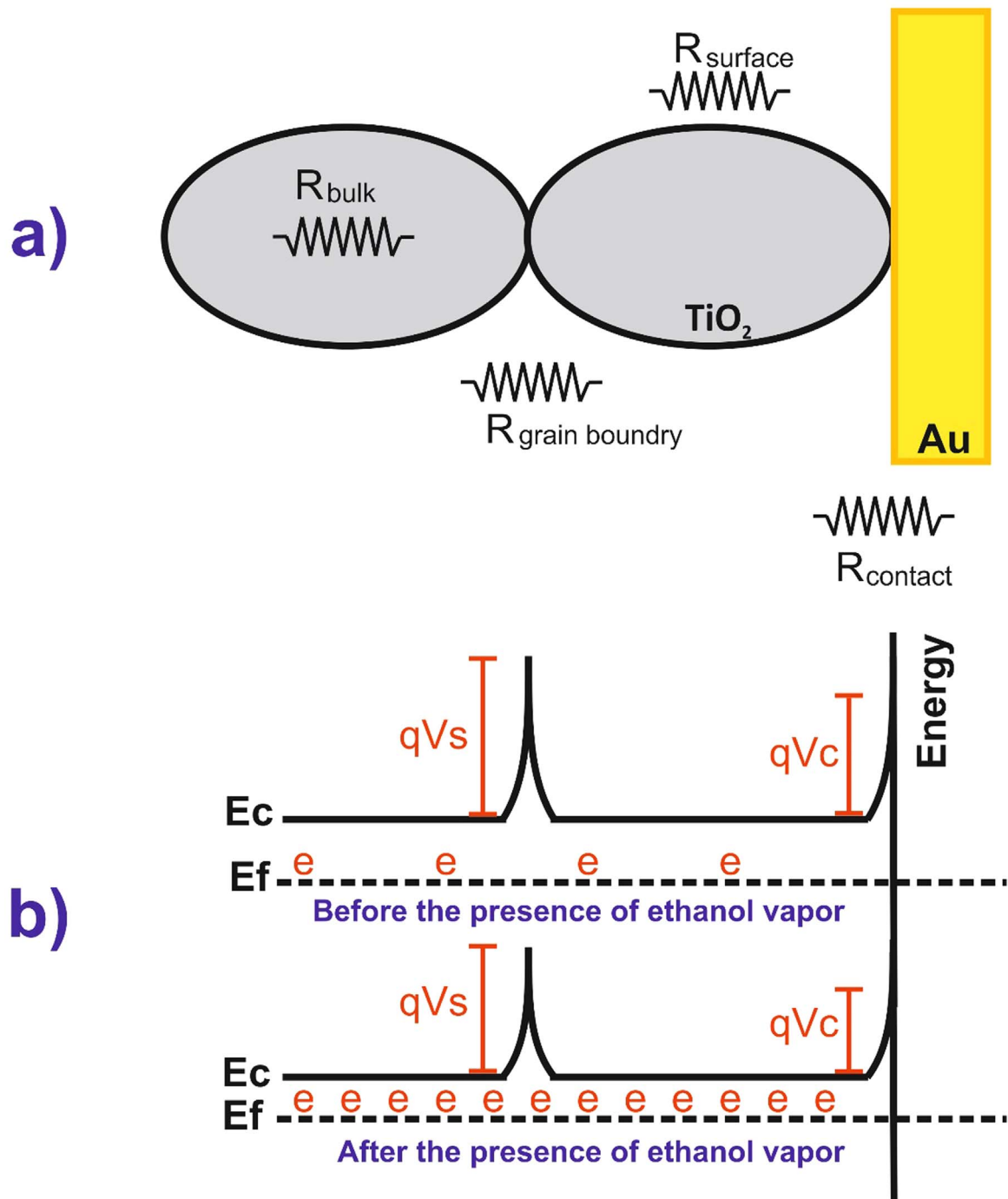


**Figure 6.** Schematic representation of (a) porous sensing layers with (b) energy bands.

diameter. As is clear from figure 2, the increase in temperature has led to an increase in porosity as well as an increase in the length of the nanowires.

XRD is used to investigate the crystal structure of the nanowires. The XRD pattern specifies the phases and sizes of the crystalline materials, thus determines the ratio of the anatase phase to the other phases in the NW- $\text{TiO}_2$ . Figure 3 presents the XRD pattern of the synthesized samples where the peaks of anatase are well recognized.

As shown in figure 3, all nanowire samples show only the anatase phases. In addition, the figure shows that the absence of spurious diffractions is a criterion to indicate crystallographic purity. Two peaks are considered for the study and using the Debye-Scherrer formula (equation 2) the grain size is calculated for the peaks. The peaks in the XRD pattern at  $2\theta = 25^\circ$  (101) and  $2\theta = 48^\circ$  (200) indicated the presence of the anatase phase. All peaks suggest that the prepared samples are in a hexagonal structure [33, 34]. The



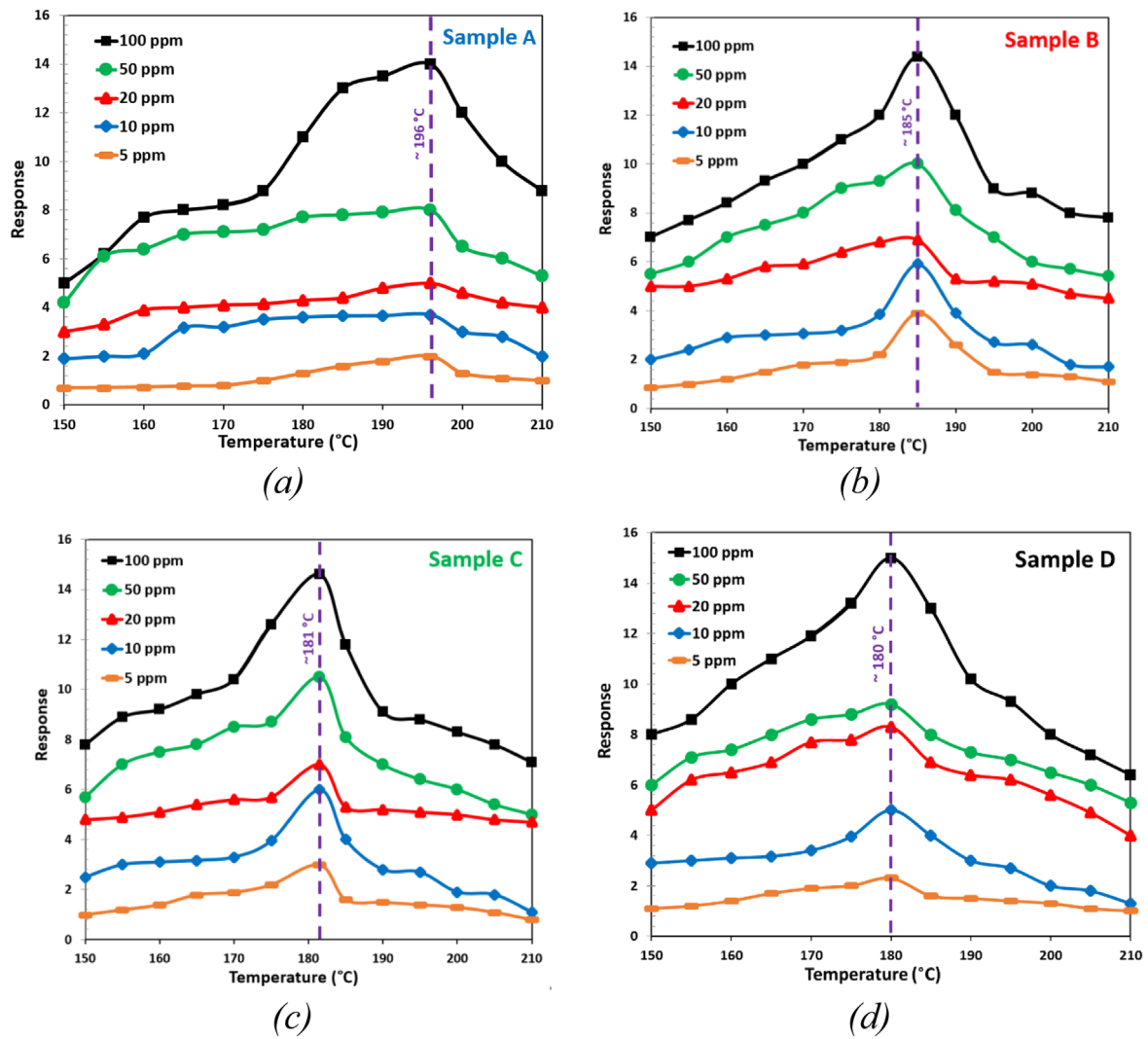


**Figure 7.** Responses of a resistive NW-TiO<sub>2</sub> gas sensor Versus operating temperature at different concentration of ethanol. (a) sample A (120 °C), (b) sample B (140 °C), (c) sample C (160 °C), (d) sample D (180 °C).

**Table 2.** Recovery and response time of NW-TiO<sub>2</sub> samples under 100 ppm ethanol vapor.

Sample	Temp (°C)	Response time (s)	Recovery time (s)	Sample	Temp (°C)	Response time (s)	Recovery time (s)
Sample A	25	330	800	Sample C	25	300	540
	150	120	220		150	90	135
	300	32	44		300	18	24
	450	29	43		450	16	21
Sample B	25	330	560	Sample D	25	310	400
	150	80	115		150	74	88
	300	26	30		300	18	22
	450	24	29		450	13	19

pattern matches well with the standard JCPDS files #21-12729 [35]. The particle diameter  $A$  is given by

$$A = 0.9 \frac{\lambda}{\beta \cos \theta}, \quad (2)$$

where  $\lambda$  is the wavelength of x-ray applied in XRD characterization ( $\lambda = 0.15405$  nm),  $\beta$  is the Full Width at Half Maximum (FWHM) and  $\theta$  is the diffraction angle.

From figure 3, considering the peak FWHM, the average particle size is calculated by using the Debye-Scherrer formula. Table 1 shows the d-spacing (Inter-planar spacing between atoms) calculated using Bragg's Law:

$$n\lambda = 2d \sin \theta, \quad (3)$$

where,  $n$  is the reflection order, which is a positive small integer (number of crystal plates). We considered  $n$  to be one.

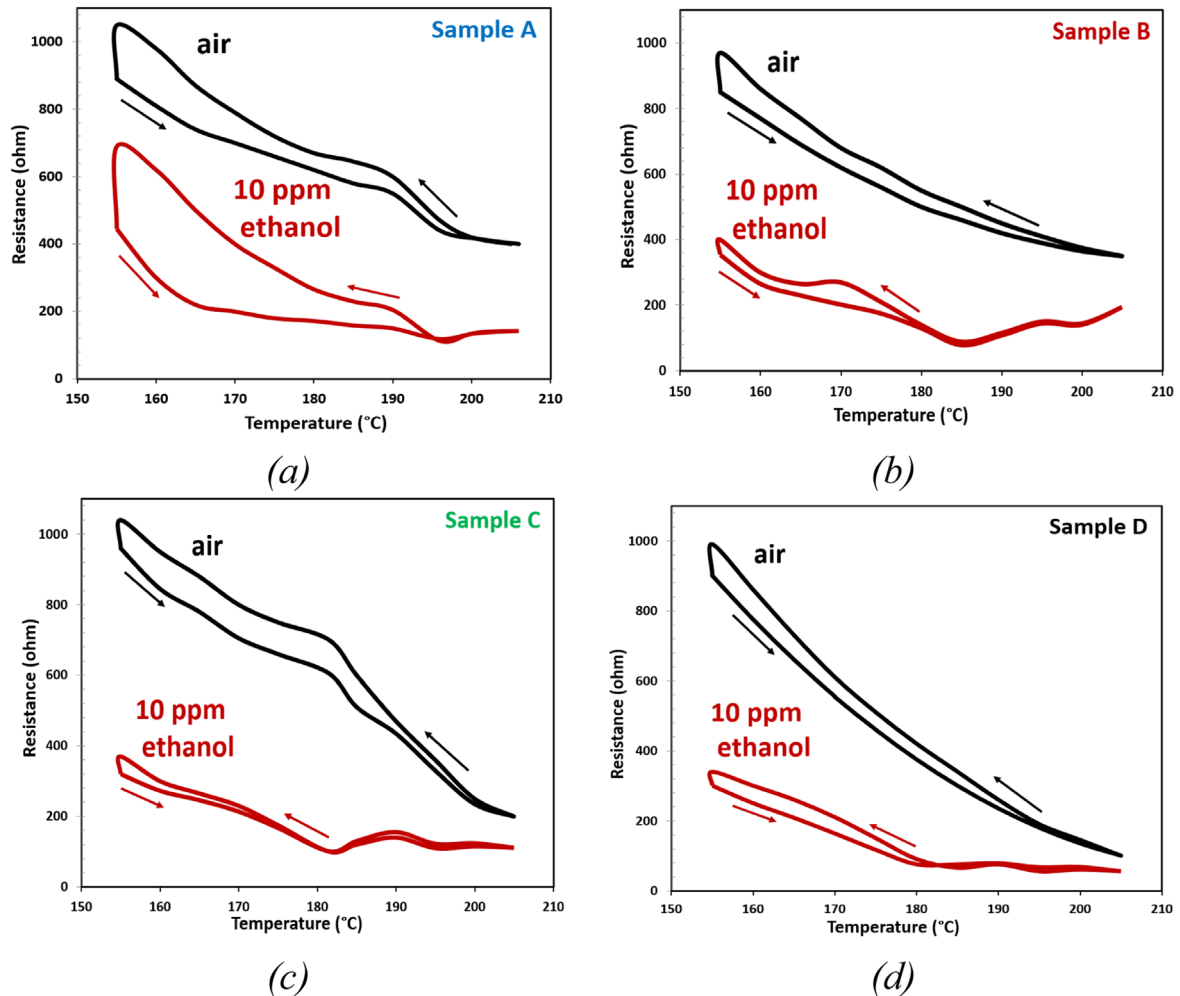


**Figure 8.** Dependence of the resistance of NW-TiO<sub>2</sub> gas sensor on temperature during the temperature modulation in synthetic air and when exposed to 10 ppm ethanol: (a) sample A (120 °C), (b) sample B (140 °C), (c) sample C (160 °C), (d) sample D (180 °C).

As can be seen from table 1, the increase in the treatment temperature did not cause significant changes in the XRD results.

The FTIR studies on the NW-TiO<sub>2</sub> samples show the characteristics of a high purity product formed with the least amount of impurities, as bands related to C–H and C–O which are typical contaminants are not observed. Figure 4 shows a sequence of FTIR spectra for NW-TiO<sub>2</sub> samples in the wavelengths varying between 500 and 4000 cm<sup>-1</sup>. All of the obtained vibrational bands are similar to those observed in the literature [36, 37]. Almost the same spectrum is observed for the four samples. It is found that TiO<sub>2</sub> nanowires with the characteristic peaks at 690 and 1620 cm<sup>-1</sup> are assigned to the Ti–O–O and Ti–O–Ti stretching vibrations, respectively. The bond –OH observed at 3440 cm<sup>-1</sup> indicates hydrogen bonding which could originate from the HCl.

### 3.2. Gas response

The gas test measurements are carried out at room temperature by recording the dynamic changes in the electrical resistance, which happens when the sample is exposed to various concentrations (5–100 ppm) of ethanol vapor in dry air. These concentrations are below the detection limit imposed on breath

analyzers [38]. The variation of the sensor performance concerning the concentration of ethanol vapor is depicted in figure 5, where the response of all four sensors increases almost linearly with the concentration. In addition, among the studied NW-TiO<sub>2</sub> samples, sample D exhibits the best performance in ethanol vapor detection.

Four different factors play roles in determining the electrical properties of gas sensing in NW-TiO<sub>2</sub> sensors: bulk resistance, surface effects, grain boundaries and the contact between the grain interface and the electrode [39–42]. As shown in figure 6(a) we can model each factor with a series resistor. The gas molecules on the surface of TiO<sub>2</sub> based on the chemical or physical adsorption/desorption can change these resistances due to the change in charge carrier concentration. The change in oxygen vacancy levels in the presence of ethanol molecules occurs in all four resistance regions. A larger porosity and higher adsorption sites can increase the sensitivity of the samples. Therefore, sample D shows a larger sensitivity. The oxygen molecules in the air are adsorbed on the grain surface. Due to the porous structure of the NW-TiO<sub>2</sub>, the oxygen molecules gradually diffuse and they eventually cover all the grains. The oxygen molecules remove the electrons from the grains during the adsorption. As shown in figure 6(b) loss of electrons may

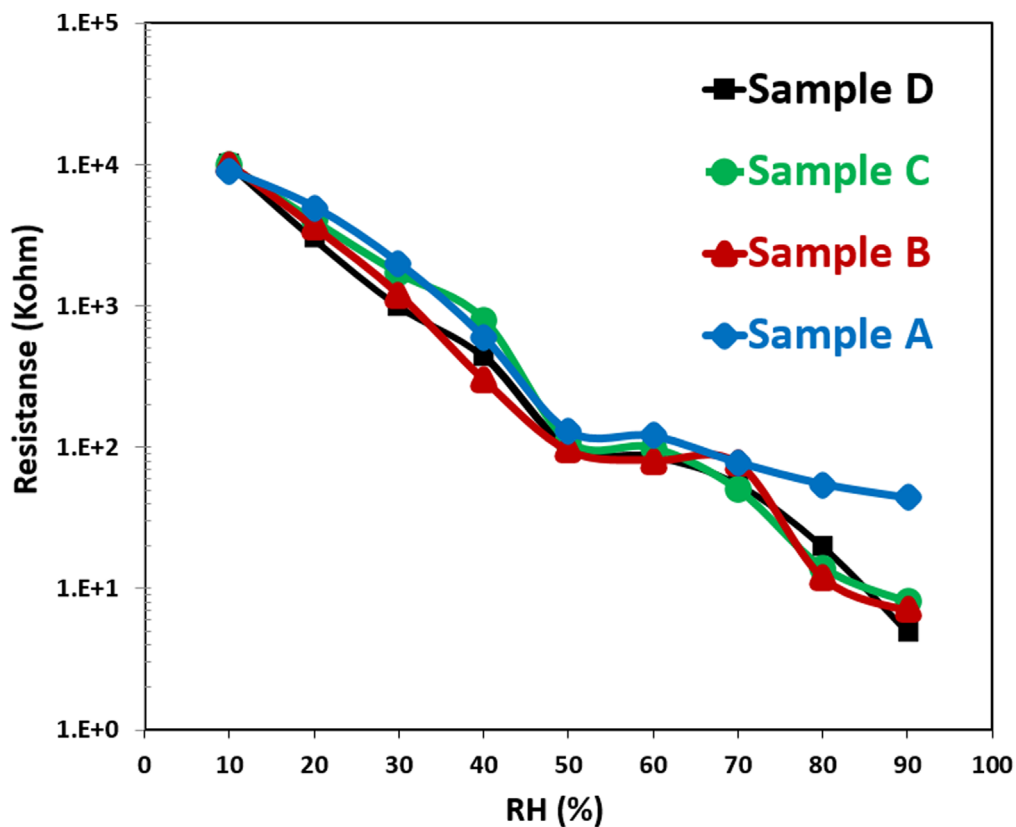
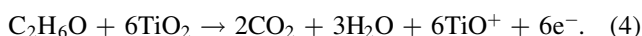


Figure 9. Relative humidity versus dc resistance plots at room temperature.

form an electron depletion layer as well as a potential barrier between grains.

It is shown in many studies (e.g., [43]) that the amount of oxygen vacancies in the  $\text{TiO}_2$  at room temperature is not sufficient for gas sensing. However, in the samples described here, due to the presence of a very large volume to surface ratio, there is a lot of surface oxygen with dangling bonds, which can be absorbed by ethanol molecules and extracted from the  $\text{TiO}_2$ . As shown in equation (4) this process can lead to the release of electrons in titanium dioxide and thus, a change in the Fermi level. When NW- $\text{TiO}_2$  is exposed to ethanol vapor, the oxyanions react with the ethanol molecules and deliver a large number of electrons to the grains. As shown in figure 6(b) these additional carriers reduce the distance between the Fermi level and the conduction band and therefore, increase the conductivity of the sample. The change in oxygen vacancy and electron distribution can also reduce the barrier between the grain boundaries and the semiconductor metal barrier.



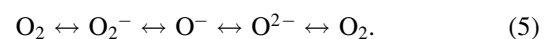
### 3.3. The effect of temperature

At a low operating temperature, a relatively low sensitivity can be expected because the gas molecules do not have sufficient thermal energy to react with the surface adsorbed oxygen species. Hence, most researchers present an optimized working temperature for  $\text{TiO}_2$  gas sensors [24, 44, 45]. Selecting an optimum

operating temperature for titanium dioxide gas sensors is thus important and its value is unchanged for various concentrations of gas. However, each structure of the  $\text{TiO}_2$  gas sensor has an optimal operating temperature. The optimum temperature for  $\text{TiO}_2$  gas sensors at temperatures above  $220^\circ\text{C}$  is reported in [46].

As shown in figure 7, the highest response is observed in the four NW- $\text{TiO}_2$  sensors at temperatures below  $200^\circ\text{C}$ . Sample D with the largest number of adsorption-desorption sites provides its maximum response at the lowest temperature. This may happen because the nanowire becomes closer to the thickness of the depletion region [47]. A larger response arises from the space-charge layer due to oxygen adsorption that penetrates deeper into the nanowires. This is because when the nanowires are close to twice the thickness of the depletion layer, the whole particle can be depleted of carriers through surface interactions, which leads to an increase of the sensing properties.

The oxygen molecules in the air environment are chemisorbed in the forms of  $\text{O}_2^-$ ,  $\text{O}^-$  and  $\text{O}^{2-}$  [48]. At a constant temperature there is a chemical equilibrium between different oxygen molecules on the surface of  $\text{TiO}_2$  and the oxygen molecule in the air:



At low temperatures, reactions with the gas molecules occur only at the surface, while at high temperatures bulk reactions between point defects in the  $\text{TiO}_2$  lattice have a larger contribution. The reduction in the response of gas sensor above  $\sim 200^\circ\text{C}$  is likely due to the difficulty in ethanol

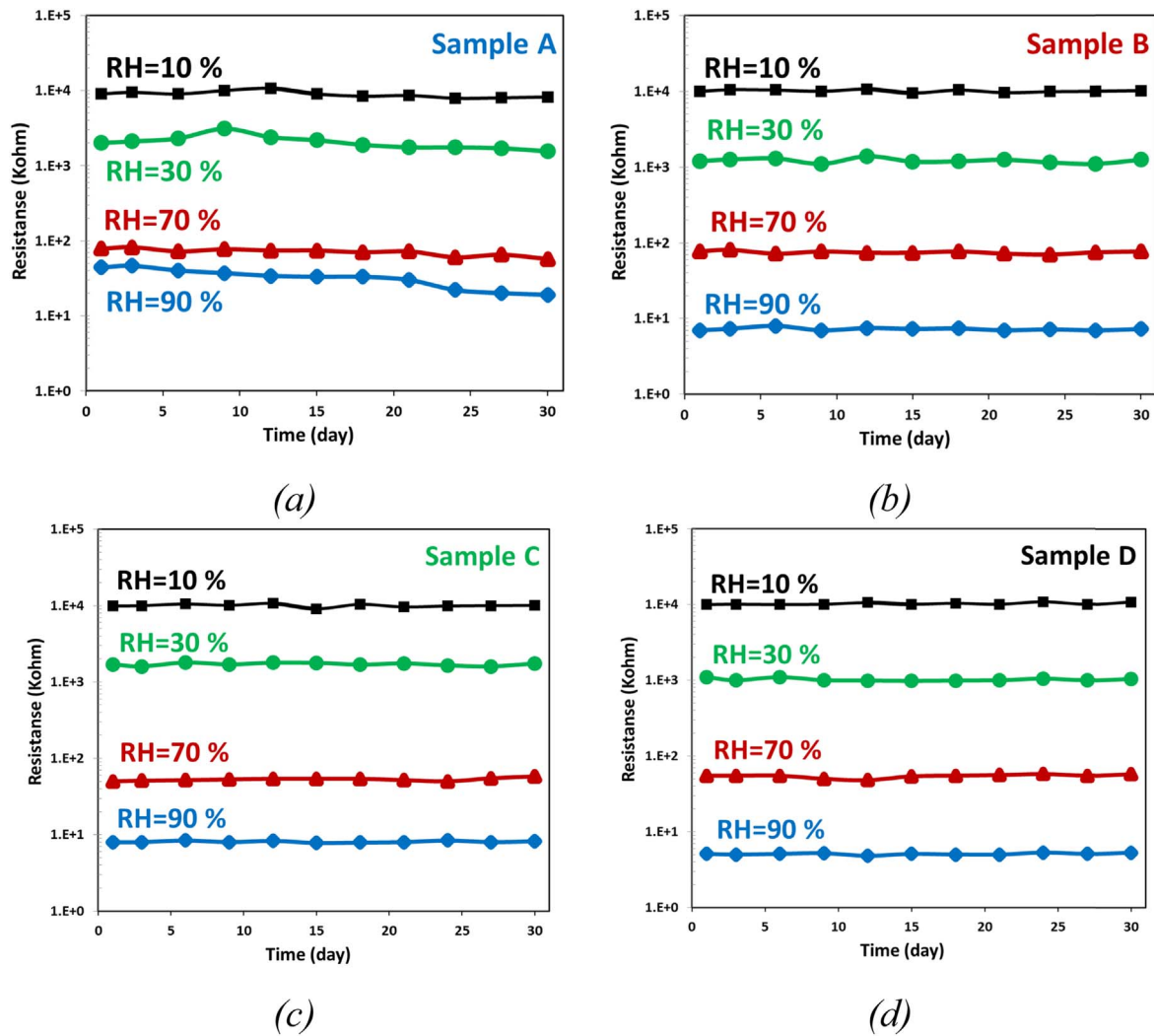


**Figure 10.** The long-term stability of NW-TiO<sub>2</sub> sensors, measured at 1V at various. RH levels: (a) sample A (120 °C), (b) sample B (140 °C), (c) sample C (160 °C), (d) sample D (180 °C) at room temperature.

gas adsorption, therefore, an optimum operating temperature should be considered to enhance the response.

The response and recovery times of our samples are decreased significantly with increasing temperature. These times do not follow a regular pattern as with the optimum response. As can be seen from table 2 they decrease with increasing temperature and then stay unchanged from about 300 °C.

Figure 8 shows the typical temperature dependencies of the actual resistance of the sensors realized with the four nanowire structures during continuous exposure to the test gas or ambient environment. One can easily observe the qualitative difference between the response of gases and the ambient air. Moreover, a large change in resistance occurs, which is due to the increased temperature. As it is clear from the figure, increasing the temperature constantly reduces the resistance of the sample but in the presence of the gas, the change in resistance is also due to the interaction with the gas molecules. Therefore, in the diagram in the presence of gas in figure 8 (red), the resistance changes become non-linear after the optimum temperature. At the optimum temperature, the

chemisorption of a gas molecule is high which indicates that the ratio of the O<sup>-</sup> and O<sup>2-</sup> species to the O<sub>2</sub><sup>-</sup> species is greatly increased. These two species are dominant at higher temperatures and frozen at the surface due to the fast temperature change. They are also much more reactive with the gas and as a result the ethanol gas response is increased [49].

Based on table 2, since the sensors have a different response and recovery time at each temperature, there exists a hysteresis curve when measuring the resistance. As the temperature increases, the response and recovery time become shorter and closer to each other. As can be seen from figure 8, sample A has the largest hysteresis.

### 3.4. The effect of humidity

The measured resistance for all samples is shown as a function of RH at room temperature in figure 9. It can be seen from the logarithmic scale over the range of 10%–90% RH that the resistance of all nanowire samples decreases strongly with increasing humidity and that the resistance of the samples varies exponentially with RH, showing a very high

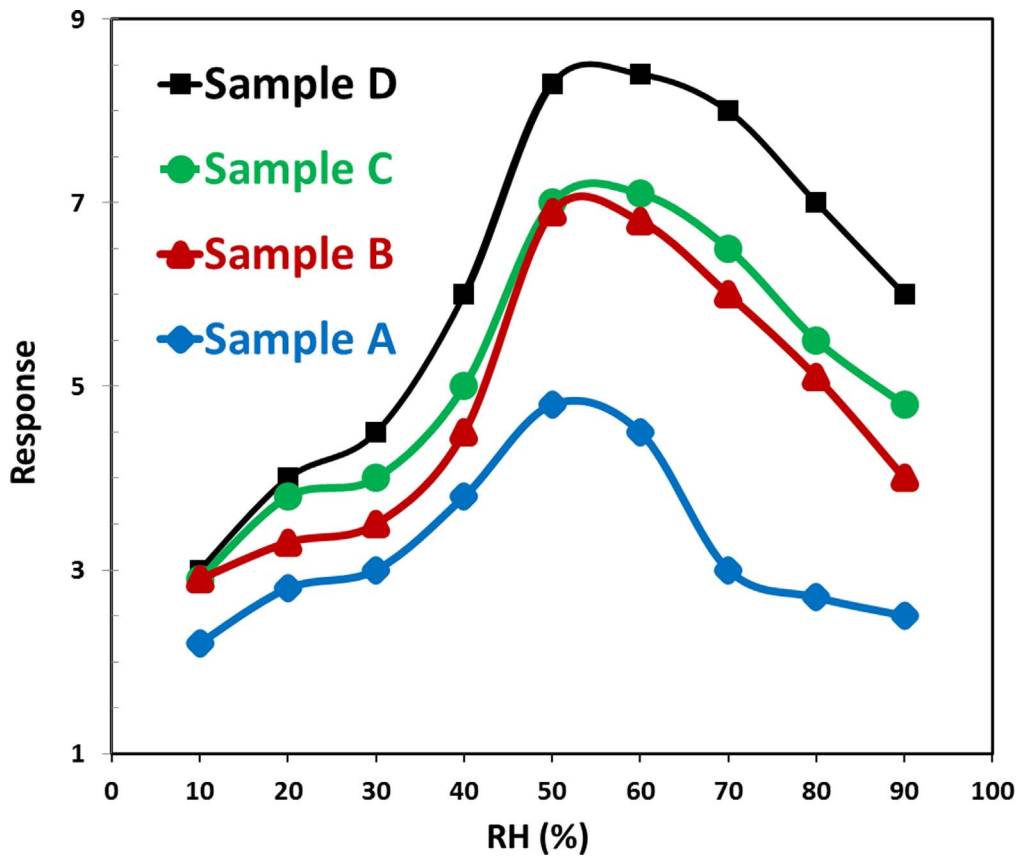


**Figure 11.** The variation of the response and the sensitivity of NW-TiO<sub>2</sub> sensors as a function of Relative Humidity (RH) during the exposure to 20 ppm ethanol at optimal operating temperature.

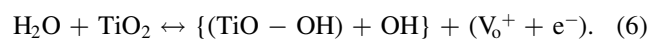
sensitivity. Between the four different samples, only minor differences are observed, with the exception of sample A at high humidity.

The stability of NW-TiO<sub>2</sub> sensors is investigated in different relative humidity's (RH). The sensing results are obtained at room temperature (25 °C) every day for two times, while kept in 10% RH, 30% RH, 70% RH and 90% RH, respectively. Figure 10 shows the effect of long-term stability. The sensor impedance has no apparent deviation for samples B, C and D over time. The resistance variation is less than 3% at each humidity region, during the time interval of 30 days. Sample A showed changes of about 50% for 90% humidity. After the stability test, the gas sensor response of the samples was re-examined. The same response curve was obtained for each experiment under different conditions, see also figure S1 (available online at [stacks.iop.org/NANO/32/325501/mmedia](https://stacks.iop.org/NANO/32/325501/mmedia)). The repeatability of the response showed that there is no serious sensing poisoning and that the sensors were fully recoverable.

To investigate the effect of humidity on the response of the fabricated sensors, ethanol vapor sensing is applied in the test chamber during a change in relative humidity. Figure 11 shows the response as a function of the applied RH to NW-TiO<sub>2</sub> samples when exposed to 20 ppm ethanol vapor. Here, the optimum operating temperature from figure 7 for each sample was applied. The effect of humidity on the conductance of metal oxide semiconductors is accepted as the

conductance increases with RH and the process is reversible [14].

The increase in the conductance of TiO<sub>2</sub> by increasing the RH can be described as a sequence of dissociation and reduction [50]. There are two types of OH groups; a rooted OH with an oxygen lattice and one bounded one with a titanium lattice:



The reaction constitutes the homolytic dissociation of H<sub>2</sub>O and the reaction of the neutral H atom with the lattice oxygen. In addition to ionizing the lattice, the reaction releases the electron as a donor to the rooted OH group.

The change in the gas sensitivity due to the presence of water molecules on the surface of titanium oxide can be the result of two factors. Firstly, free carrier changes and interaction between both the hydroxyl group and the hydrogen atom originating from the water molecule with a gas molecule group. Secondly, co-adsorption of water on the adsorption of another adsorbate could play a role as an electron acceptor [51].

Consequently, H<sub>2</sub>O molecules provide the necessary conditions for oxygen adsorption, electrons, and oxygen vacancies. Water absorption can then accelerate the absorption of oxygen. Thus, due to the surface distribution and coverage of hydroxyl groups and the presence of oxygen species, an enhancement or reduction effect of RH may happen on the conductance in the response to ethanol. As it is

clear in figure 11 there are fewer hydroxyl groups and oxygen on the surface of nanowires at low relative humidity, which leads to a weak response of the sensors.

When humidity increases to about 60% RH, the change in the hydroxyl groups is smaller than that of oxygen on the surface. Therefore, it continues to increase the response. When the humidity is too high, the hydroxyl groups OH cover almost the surface and limit the oxygen adsorption. Now, according to equations (4) and (6), the absorption of water and ethanol increases electron carriers. Therefore, in high humidity, the number of electrons released due to water molecule absorption is considerably high such that the effect of electrons due to the absorption of ethanol gas is less observed.

The effect of relative humidity and temperature on the selectivity of fabricated gas sensors was examined for some gases such as other volatile organic compounds and ammonia but no meaningful relationship between selectivity of fabricated sensor and these two parameter changes has been observed.

#### 4. Conclusion

We studied the effects of humidity and temperature on the response of titanium dioxide nanowire to ethanol vapor. We employed the growth of TiO<sub>2</sub> nanowires via the hydrothermal method as a simple and low-cost fabrication method. In the growth process of titanium dioxide, four different treatment temperatures were used to obtain different morphologies of nanowires. Gas sensing results showed that the sample with high porosity and longer wire length was more sensitive to ethanol vapor than other samples. The ethanol vapor sensing characteristics as a function of temperature were investigated. We found that by increasing the treatment temperature in the growth process the maximum sensitivity shifts towards a lower operating temperature.

In the case that both gas and water molecules are presented simultaneously in the test chamber, low humidity increased the sensitivity to ethanol. In contrast, at high humidity we observed competitive sorption and reduction of the ethanol sensing response of the sensors. Thus far in the study, we showed that the influence of humidity and temperature on the sensor response can be evaluated by the morphology of the nanowires that can be changed in the growth process. Future studies will focus on the synthesis and the use of highly hydrophobic TiO<sub>2</sub> that sorb alcohols vapor more selectively than water to improve the sensor insensitivity to humidity.

#### Data availability statement

All data that support the findings of this study are included within the article (and any supplementary files).

#### ORCID iDs

Mostafa Shooshtari  <https://orcid.org/0000-0003-1292-0683>

Sten Vollebregt  <https://orcid.org/0000-0001-6012-6180>

#### References

- [1] Karlsson M C *et al* 2012 Characterisation of silicon, zirconium and aluminium coated titanium dioxide pigments recovered from paint waste *Dyes Pigm.* **162** 145–52
- [2] Aboulouard A *et al* 2020 Dye sensitized solar cells based on titanium dioxide nanoparticles synthesized by flame spray pyrolysis and hydrothermal sol–gel methods: a comparative study on photovoltaic performances *J. Mater. Res. Technol.* **9** 1569–77
- [3] Klestova A, Cheplagin N, Keller K, Slabov V, Zaretskaya G and Vinogradov A V 2019 Inkjet printing of optical waveguides for single-mode operation *Adv. Opt. Mater.* **7** 1801113
- [4] Schneider S L and Lim H W 2019 A review of inorganic UV filters zinc oxide and titanium dioxide *Photodermatol., Photoimmunol. Photomed.* **35** 442–6
- [5] Rzajj J M and Abass A M 2020 Review on: TiO<sub>2</sub> thin film as a metal oxide gas sensor *J. Chem. Rev.* **2** 114–21
- [6] Xue X *et al* 2012 Raman investigation of nanosized TiO<sub>2</sub>: effect of crystallite size and quantum confinement *J. Phys. Chem. C* **116** 8792–7
- [7] Hmiel A and Xue Y 2012 Quantum confinement and surface relaxation effects in rutile TiO<sub>2</sub> nanowires *Phys. Rev. B* **85** 235461
- [8] Shen S *et al* 2018 Titanium dioxide nanostructures for photoelectrochemical applications *Prog. Mater. Sci.* **98** 299–385
- [9] Chen X and Selloni A 2014 Introduction: titanium dioxide (TiO<sub>2</sub>) nanomaterials *Chemical reviews* **114** 9281–2
- [10] Taha S *et al* 2020 Titanium dioxide nanostructure based alcohol vapor sensor *AIP Conf. Proc.* p 020195
- [11] Hazra A, Dutta K, Bhowmik B, Chattopadhyay P and Bhattacharyya P 2014 Room temperature alcohol sensing by oxygen vacancy controlled TiO<sub>2</sub> nanotube array *Appl. Phys. Lett.* **105** 081604
- [12] Dey A 2018 Semiconductor metal oxide gas sensors: a review *Mater. Sci. Eng. B* **229** 206–17
- [13] Ji H, Zeng W and Li Y 2019 Gas sensing mechanisms of metal oxide semiconductors: a focus review *Nanoscale* **11** 22664–84
- [14] Wang C, Yin L, Zhang L, Xiang D and Gao R 2010 Metal oxide gas sensors: sensitivity and influencing factors *Sensors* **10** 2088–106
- [15] Shooshtari M, Salehi A and Vollebregt S 2021 Effect of humidity on gas sensing performance of carbon nanotube gas sensors operated room temperature *IEEE Sens. J.* **21** 5763–70
- [16] Gaman V, Anisimov O, Maksimova N, Sergeichenko N, Sevast'yanov E Y and Chernikov E 2008 The effect of water vapor on the electrical properties and sensitivity of thin-film gas sensors based on tin dioxide *Russ. Phys. J.* **51** 831–9
- [17] Tian W-C, Ho Y-H, Chen C-H and Kuo C-Y 2013 Sensing performance of precisely ordered TiO<sub>2</sub> nanowire gas sensors fabricated by electron-beam lithography *Sensors* **13** 865–74
- [18] Giannakoudakis D A, Chatel G and Colmenares J C 2020 Mechanochemical forces as a synthetic tool for zero- and one-dimensional titanium oxide-based nano-photocatalysts *Top. Curr. Chem.* **378** 2

- [19] Lashkov A V *et al* 2020 The Ti wire functionalized with inherent TiO<sub>2</sub> nanotubes by anodization as one-electrode gas sensor: a proof-of-concept study *Sensors Actuators B* **306** 127615
- [20] Zhao G *et al* 2020 *In situ* growing double-layer TiO<sub>2</sub> nanorod arrays on new-type FTO electrodes for low-concentration NH<sub>3</sub> detection at room temperature *ACS Appl. Mater. Interfaces* **12** 8573–82
- [21] Hu P *et al* 2010 Enhancement of ethanol vapor sensing of TiO<sub>2</sub> nanobelts by surface engineering *ACS Appl. Mater. Interfaces* **2** 3263–9
- [22] Munasinghe Arachchige H M, Zappa D, Poli N, Gunawardhana N, Attanayake N H and Comini E 2020 Seed-assisted growth of TiO<sub>2</sub> nanowires by thermal oxidation for chemical gas sensing *Nanomaterials* **10** 935
- [23] Ramgir N *et al* 2020 TiO<sub>2</sub>/ZnO heterostructure nanowire based NO<sub>2</sub> sensor *Mater. Sci. Semicond. Process.* **106** 104770
- [24] Yang X *et al* 2019 Enhanced gas sensing performance based on the fabrication of polycrystalline Ag@ TiO<sub>2</sub> core-shell nanowires *Sensors Actuators B* **286** 483–92
- [25] Zhou M, Liu Y, Wu B and Zhang X 2019 Different crystalline phases of aligned TiO<sub>2</sub> nanowires and their ethanol gas sensing properties *Physica E* **114** 113601
- [26] Shi J and Wang X 2011 Growth of rutile titanium dioxide nanowires by pulsed chemical vapor deposition *Cryst. Growth Des.* **11** 949–54
- [27] Li L, Qin X, Wang G, Qi L, Du G and Hu Z 2011 Synthesis of anatase TiO<sub>2</sub> nanowires by modifying TiO<sub>2</sub> nanoparticles using the microwave heating method *Appl. Surf. Sci.* **257** 8006–12
- [28] Ashkarran A 2011 Metal and metal oxide nanostructures prepared by electrical arc discharge method in liquids *J. Cluster Sci.* **22** 233
- [29] Nechache R, Nicklaus M, Diffalah N, Ruediger A and Rosei F 2014 Pulsed laser deposition growth of rutile TiO<sub>2</sub> nanowires on Silicon substrates *Appl. Surf. Sci.* **313** 48–52
- [30] Mohammad S N 2008 Analysis of the vapor-liquid-solid mechanism for nanowire growth and a model for this mechanism *Nano Lett.* **8** 1532–8
- [31] Al-Hajji L *et al* 2020 Impact of calcination of hydrothermally synthesized TiO<sub>2</sub> nanowires on their photocatalytic efficiency *J. Mol. Struct.* **1200** 127153
- [32] Schneider C, Liu N, Romeis S, Peukert W and Schmuki P 2019 Easy room temperature synthesis of high surface area anatase nanowires with different morphologies *ChemistryOpen* **8** 817–21
- [33] Zhu S, Jiang J, Zhang X, Liang Y, Cui Z and Yang X 2017 Novel nanosized anatase TiO<sub>2</sub> hexagonal prism filled with nanoporous structure *Mater. Des.* **116** 238–45
- [34] Dai S, Wu Y, Sakai T, Du Z, Sakai H and Abe M 2010 Preparation of highly crystalline TiO<sub>2</sub> nanostructures by acid-assisted hydrothermal treatment of hexagonal-structured nanocrystalline titania/cetyltrimethylammonium bromide nanoskeleton *Nanoscale Res. Lett.* **5** 1829–35
- [35] Theivasanthi T and Alagar M 2013 Titaniumdioxide (TiO<sub>2</sub>) nanoparticles XRD analyses: an insight *Cornel University Library* arXiv:1307.1091
- [36] Bagheri S, Shamel K and Abd Hamid S B 2013 Synthesis and characterization of anatase titanium dioxide nanoparticles using egg white solution via Sol–Gel method *Journal of Chemistry* **2013** 848205
- [37] León A *et al* 2017 FTIR and Raman characterization of TiO<sub>2</sub> nanoparticles coated with polyethylene glycol as carrier for 2-methoxyestradiol *Appl. Sci.* **7** 49
- [38] Brousse T and Schleich D 1996 Sprayed and thermally evaporated SnO<sub>2</sub> thin films for ethanol sensors *Sensors Actuators B* **31** 77–9
- [39] Ponzoni A *et al* 2017 Metal oxide gas sensors, a survey of selectivity issues addressed at the SENSOR Lab, Brescia (Italy) *Sensors* **17** 714
- [40] Sun Y-F *et al* 2012 Metal oxide nanostructures and their gas sensing properties: a review *Sensors* **12** 2610–31
- [41] Kirner U *et al* 1990 Low and high temperature TiO<sub>2</sub> oxygen sensors *Sensors Actuators B* **1** 103–7
- [42] Lee J-S, Katoch A, Kim J-H and Kim S S 2016 Growth of networked TiO<sub>2</sub> nanowires for gas-sensing applications *J. Nanosci. Nanotechnol.* **16** 11580–5
- [43] Ramanavicius S and Ramanavicius A 2020 Insights in the application of stoichiometric and non-stoichiometric titanium oxides for the design of sensors for the determination of gases and VOCs (TiO<sub>2-x</sub> and Ti<sub>n</sub>O<sub>2n-1</sub> versus TiO<sub>2</sub>) *Sensors* **20** 6833
- [44] Guo W, Feng Q, Tao Y, Zheng L, Han Z and Ma J 2016 Systematic investigation on the gas-sensing performance of TiO<sub>2</sub> nanoplate sensors for enhanced detection on toxic gases *Mater. Res. Bull.* **73** 302–7
- [45] Tong X, Shen W, Zhang X, Corriou J-P and Xi H 2020 Synthesis and density functional theory study of free-standing Fe-doped TiO<sub>2</sub> nanotube array film for H<sub>2</sub>S gas sensing properties at low temperature *J. Alloys Compd.* **832** 155015
- [46] Karunakaran B, Uthirakumar P, Chung S, Velumani S and Suh E-K 2007 TiO<sub>2</sub> thin film gas sensor for monitoring ammonia *Mater. Charact.* **58** 680–4
- [47] Park S-H, Ryu J-Y, Choi H-H and Kwon T-H 1998 Zinc oxide thin film doped with Al<sub>2</sub>O<sub>3</sub>, TiO<sub>2</sub> and V<sub>2</sub>O<sub>5</sub> as sensitive sensor for trimethylamine gas *Sensors Actuators B* **46** 75–9
- [48] Chachuli S A M, Hamidon M N, Ertugrul M, Mamat M S, Jaafar H and Shamsudin N 2020 TiO<sub>2</sub>/B<sub>2</sub>O<sub>3</sub> thick film gas sensor for monitoring carbon monoxide at different operating temperatures *Journal of Physics: Conf. Series* p 012040
- [49] Heilig A, Barsan N, Weimar U, Schweizer-Berberich M, Gardner J and Göpel W 1997 Gas identification by modulating temperatures of SnO<sub>2</sub>-based thick film sensors *Sensors Actuators B* **43** 45–51
- [50] Wang Y, Zhou Y and Wang Y 2020 Humidity activated ionic-conduction formaldehyde sensing of reduced graphene oxide decorated nitrogen-doped MXene/titanium dioxide composite film *Sensors Actuators B* **323** 128695
- [51] Henrich V E and Cox P A 1996 *The Surface Science of Metal Oxides* (Cambridge: Cambridge University Press)